Inorg. Chem. **2005**, *44*, 8076–8086

Ground-State Electronic and Magnetic Properties of a μ_3-Oxo-Bridged Trinuclear Cu(II) Complex: Correlation to the Native Intermediate of the Multicopper Oxidases

Jungjoo Yoon and Edward I. Solomon*

Department of Chemistry, Stanford University, Stanford, California 94305

Received May 16, 2005

The ground-state electronic and magnetic properties of one of the possible structures of the trinuclear Cu^{II} site in the native intermediate (NI) of the multicopper oxidases, the μ_3-oxo-bridged structure, are evaluated using the C_3-symmetric Cu_3^{II} complex, μ_3O. μ_3O is unique in that no ligand, other than the oxo, contributes to the exchange coupling. However, μ_3O has a ferromagnetic ground state, inconsistent with that of NI. Therefore, two perturbations have been considered: protonation of the μ_3-oxo ligand and relaxation of the μ_3-oxo ligand into the Cu_3 plane. Notably, when the oxo ligand is sufficiently close to the Cu_3 plane (<0.3 Å), the ground state of μ_3O becomes antiferromagnetic and can be correlated to that of NI. In addition, the ferromagnetic ^4A ground state of μ_3O is found from variable-temperature EPR to undergo a zero-field splitting (ZFS) of $2D = -5.0$ cm^{-1}, which derives from the second-order anisotropic exchange. This allows evaluation of the σ-to-π excited-state exchange pathways and provides experimental evidence that the orbitally degenerate ^2E ground state of the antiferromagnetic μ_3O would also undergo a ZFS by the first-order antisymmetric exchange that has the same physical origin as the anisotropic exchange. The important contribution of the μ_3-oxo bridge to the ground-to-ground and ground-to-excited-state superexchange pathways that are responsible for the isotropic, antisymmetric, and anisotropic exchanges are discussed.

Introduction

Trimeric copper complexes with trigonal symmetry have attracted significant interest as these complexes resemble the active sites of the multicopper oxidases (MCOs), which include laccase, ascorbate oxidase, and ceruloplasmin.[1] The fully reduced forms of these enzymes react with O_2 to form the native intermediate (NI) that has a fully oxidized antiferromagnetically coupled trinuclear Cu^{II} cluster in which all Cu centers are bridged by the product of full O_2 reduction.[2] It has been suggested that the bridged structure results in new signals in the electron paramagnetic resonance (EPR) spectrum with g values of 2.15, 1.86, and 1.65, the latter two being < 2.0.[2] In addition, a low-lying excited doublet state exists ~150 cm^{-1} above the ground doublet state as determined from EPR power saturation and variable-temperature (VT) magnetic circular dichroism (MCD) spectroscopies.[2]

Chart 1. Proposed Structures of the Native Intermediate

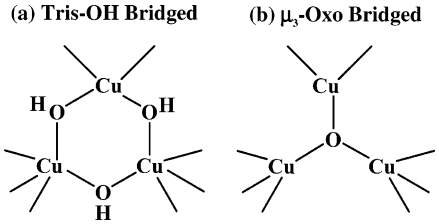

Two limiting structures for the trinuclear Cu^{II} site in NI are consistent with its reactivity and spectral features.[1,2] The first structure has three μ_2-OH ligands, each bridging a Cu^{II} pair where two OH^- ligands derive from O_2 and the third from an ambient H_2O (Chart 1a); the second structure has a single μ_3-oxo ligand bridging all three Cu^{II} centers of the cluster with the second O atom from O_2 reduction, either remaining bound or dissociated from the trinuclear site (Chart 1b). Recently, we have reported the ground-state properties

* Author to whom correspondence should be addressed. E-mail: edward.solomon@stanford.edu.

(1) (a) Solomon, E. I.; Chen, P.; Metz, M.; Lee, S.-K.; Palmer, A. E. *Angew. Chem., Int. Ed.* **2001**, *40*, 4570−4590. (b) Solomon, E. I.; Sundaram, U. M.; Machonkin, T. E. *Chem. Rev.* **1996**, *96*, 2563−2605. (c) Solomon, E. I.; Baldwin, M. J.; Lowery, M. D. *Chem. Rev.* **1992**, *92*, 521−542.

(2) Lee, S.-K.; DeBeer, G. S.; Antholine, W. E.; Hedman, B.; Hodgson, K. O.; Solomon, E. I. *J. Am. Chem. Soc.* **2002**, *124*, 6180−6193.

10.1021/ic0507870 CCC: $30.25
Published on Web 09/20/2005

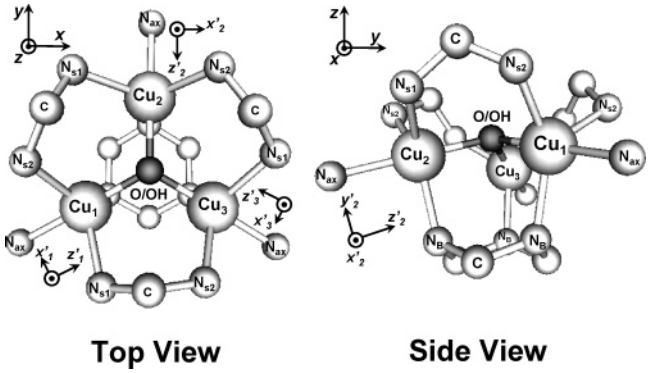

Figure 1. μ_3O/μ_3OH models used in the DFT calculations (H atoms not shown) with the molecular (x, y, and z) and the local coordinate axes (x', y', and z') indicated. The ethylene links in the bowl-shaped macrocyclic ligand were truncated with H atoms for simplification. Refer to Scheme S1 (Supporting Information) for the full structure of the N ligand.

of the first structure using a D_3 symmetric model complex, TrisOH.[3,4] In TrisOH, all Cu^{II} pairs are antiferromagnetically coupled, yielding a ^{2}E ground state with a zero-field splitting (ZFS) of 65 cm^{-1}. Moreover, a strongly anisotropic EPR signal, which shifts in resonance field with g_{eff} values from 2.32 to ~1.2, was observed in the single-crystal EPR spectrum.[3] These characteristic features of the ^{2}E ground state of TrisOH arise from the combined effect of symmetry lowering, which reflects a magnetic Jahn−Teller distortion, and antisymmetric exchange,[5] which results from first-order spin−orbit coupling (SOC) to an excited state and excited-to-ground-state superexchange interactions. In particular, the low g_{eff} values < 2.0 are due to the antisymmetric exchange, which allows field-induced mixing between the two ZFS doublets of the ^{2}E ground state when the molecular z axis (normal to the Cu_3 plane) is oriented perpendicular to the magnetic field.[6] We have shown that the structure of TrisOH is well-suited for antisymmetric exchange as it provides efficient local $d_{x^2-y^2}$-to-d_{xy} SOC as well as the pathways for ground-to-excited-state superexchange interactions between the $d_{x^2-y^2}$ ground state of one Cu center with the d_{xy} excited state of another Cu center through the Cu−OH σ bonds.[3]

The ground-state properties of the second possible structure of NI can be best studied using the C_3-symmetric Cu_3^{II} complex (μ_3O, Figure 1) synthesized by Suh et al.[7] μ_3O is the only μ_3-oxo-bridged Cu_3^{II} complex without other effective bridging ligands, such as pyrazolates,[8] that may significantly affect the exchange coupling.[9] The distances between the Cu^{II} centers of the two neighboring trimer units is large enough (closest being 9.67 Å) to avoid significant intermolecular interactions. Moreover, μ_3O exists in a protonated form, μ_3OH, that has been also determined to be C_3 symmetric. Thus, the bonding interactions between the μ_3-oxo ligand and the Cu^{II} centers can be greatly simplified, and the protonated μ_3OH form can be used as a perturbation of the μ_3O structure. However, μ_3O has a ferromagnetic ^{4}A ground state ($J = +54.5$ cm^{-1}),[7] inconsistent with the ground state of NI. A possible reason for this difference is that the oxo ligand lies ~0.5 Å above the Cu_3 plane in μ_3O. However, as the trinuclear Cu^{II} site in NI has a more flexible ligand environment, the oxo ligand is expected to be less protruded above the Cu_3 plane than in μ_3O, which has a relatively rigid, bowl-shaped macrocyclic ligand.[10]

This study focuses on the ground-state electronic and magnetic properties of the μ_3O structure. First, the Cu−O bonding interactions in the ferromagnetic μ_3O and its protonated form, μ_3OH, are evaluated using the combination of EPR spectroscopy and DFT calculations. Then, a set of DFT calculations evaluating the effect of the position of the oxo ligand relative to the Cu_3 plane is presented, which allows correlation to the anitiferromagnetic ground state of NI. In addition, the orbitally nondegenerate ^{4}A ground state of μ_3O can zero-field split into $M_S = \pm^1/_2$ and $\pm^3/_2$ doublets via SOC that derives from second-order anisotropic exchange (see below). As the anisotropic exchange shares the same physical origin as the antisymmetric exchange, the evaluation of the contributions of the μ_3-oxo bridging ligand to both the ground-to-ground and ground-to-excited-state superexchange interactions would provide insight into the ground-state properties of both the ferromagnetically and antiferromagnetically coupled μ_3-oxo-bridged trimeric Cu^{II} systems and allow extension to the ground-state properties of NI.

Experimental Section

Detailed descriptions of the syntheses, crystal structures, and magnetic susceptibilities of μ_3O and its protonated form, μ_3OH, are as reported.[7]

EPR spectra were obtained using a Bruker EMX spectrometer. For X-/Q-band experiments, Bruker ER 041XG/ER 051QR microwave bridges and ER 4102ST/ER 5106QT cavities were used. Temperatures from 3.65 to 120 K were maintained using an Oxford ITC503 temperature controller with an ESR 900 continuous flow cryostat for X-band and a CF935 dynamic continuous flow cryostat

(3) Yoon, J.; Mirica, L. M.; Stack, T. D. P.; Solomon, E. I. *J. Am. Chem. Soc.* **2004**, *126*, 12586−12595.
(4) Mirica, L. M.; Stack, T. D. P. *Inorg. Chem.* **2005**, *44*, 2131−2133.
(5) (a) Moriya, T. *Phys. Rev.* **1960**, *120*, 91−98. (b) Moriya, T. In *Magnetism*; Rado, G. T., Suhl, H., Eds.; Academic Press: New York, 1963; Vol. 1, pp 85−125. (c) Dzyaloshinsky, I. *J. Phys. Chem. Solids* **1958**, *4*, 241−255. (d) Gatteschi, D.; Bencini, A. In *Magneto-Structural Correlations in Exchange Coupled Systems*; Willett, R. D., Gatteschi, D., Kahn, O., Eds.; D. Reidel: Dordrecht, The Netherlands, 1985; pp 241−268. (e) Bencini, A.; Gatteschi, D. *Electron Paramagnetic Resonance of Exchange Coupled Systems*; Springer-Verlag: Berlin, 1990.
(6) Tsukerblat, B. S.; Belinskii, M. I.; Fainzil'berg, V. E. *Sov. Sci. Rev., Sect. B* **1987**, *9*, 337−481.
(7) Suh, M. P.; Han, M. Y.; Lee, J. H.; Min, K. S.; Hyeon, C. *J. Am. Chem. Soc.* **1998**, *120*, 3819−3820.
(8) (a) Angaridis, P. A.; Baran, P.; Boča, R.; Cervantes-Lee, F.; Haase, W.; Mezei, G.; Raptis, R. G.; Werner R. *Inorg. Chem.* **2002**, *41*, 2219−2228. (b) Butcher, R. J.; O'Conner, C. J.; Sinn, E. *Inorg. Chem.* **1981**, *20*, 537−545.
(9) In the Cu_3 complexes of ref 8, the additional N=N bridging ligands from the pyrazolates are in the same plane as the magnetic orbitals (Cu $d_{x^2-y^2}$). Also, the conjugate π bonds of the N=N would be relatively close in energy to the metal d orbitals. These conditions would promote effective electron delocalization and spin polarization, and thus, the exchange coupling in these Cu_3 complexes would be considerably affected by the N=N bonds. On the other hand, the N−CH_2−N bridging ligands in the μ_3O/μ_3OH model complexes are not in the same plane as the magnetic orbitals (Cu d_{z^2}) and the saturated methylene bridges (−CH_2−) have very stable occupied orbitals with larger energy gaps to the metal d orbitals. Therefore, contribution of the N−CH_2−N bridging ligands to the exchange coupling in μ_3O/μ_3-OH would be very limited.
(10) The full structure of the macrocyclic ligand is given in the Supporting Information (Scheme S1).

for Q-band experiments (transfer line GFS650 from Oxford Instruments). The powder samples were prepared anaerobically by finely grinding the single crystals of μ_3O and μ_3OH under a N_2 atmosphere in a glovebox. EPR spectra were baseline subtracted and simulated using XSophe (Brüker).[11]

Spin-unrestricted DFT calculations were performed using Gaussian 98[12] and Amsterdam Density Functional (ADF)[13] programs, and the results were analyzed using AOMix.[14] All geometry optimizations were performed at uB3LYP/Lanl2dz level.[15] For both μ_3O and μ_3OH, all the ethylene groups linking N atoms in the macrocyclic ligand were truncated with H atoms (Figure 1) and geometry optimized in C_3 symmetry with $\langle S^2 \rangle \approx 3.75$. The resulting geometries were then used for single-point calculations with a triple-ζ Slater-type orbital basis set (ADF basis set TZP) with a single polarization function at the local density approximation of Vosko, Wilk, and Nusair[16] with nonlocal gradient corrections of Becke and Perdew.[17]

Results

Electron Paramagnetic Resonance. (a) μ_3O. The EPR spectra of the powder μ_3O sample taken at the X-band (9.390 GHz = 0.313 cm^{-1}, 8 K) and the Q-band (33.81 GHz = 1.13 cm^{-1}, 10 K) are presented with their simulated spectra in Figure 2. The EPR signals in X-band are observed only below 120 K, and their intensities reach their maxima near 8 K. No change in the spectral shape is observed over the temperature range of 3.73−120 K (Figure S1, Supporting Information). Two transitions at g_{eff} of 3.64 and 2.06 in X-band and 3.77 and 2.06 in Q-band are observed with no discernible hyperfine feature. These transitions correspond to the "$g = 4$" and "$g = 2$" resonances of an axial zero-field split quartet ($S_{\text{tot}} = {}^3/_2$) system demonstrating a ferromagnetic ground state, consistent with magnetic susceptibility data[7] (the energy level is shown in Scheme 1). If the two Kramers doublets originating from the ZFS of the ^{4}A ground state are well-separated in energy, such that the intermixing of these states can be ignored, then the $g_{\text{eff}} \sim 4$ resonance is equal to twice the true $g_{x,y}$ of the molecule, which, in turn, corresponds to the vector-coupled g values

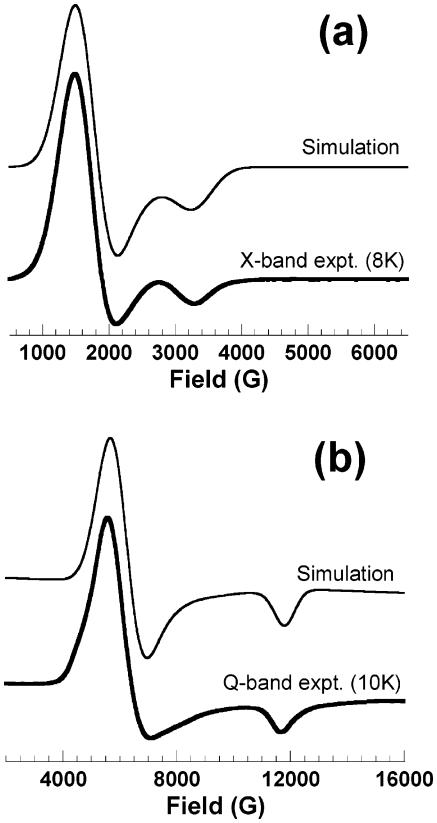

Figure 2. EPR spectra of powder μ_3O complex and their simulations using $g_x = g_y = 2.021$, $g_z = 2.064$, $D = -2.50$ cm^{-1}, $E/D = 0$, line width parameters $W_{x,y,z} = (650, 650, 280$ G), and the ZFS $D-E$ strain parameters σ_D and $\sigma_E = 0.06$ and 0.07, respectively. (a) X-band spectrum taken at 0.3 mW, 8.0 K, and 9.390 GHz and (b) Q-band EPR spectrum at 0.097 mW, 10.0 K, and 33.81 GHz.

Scheme 1. Ground-State Energy Diagram of μ_3O

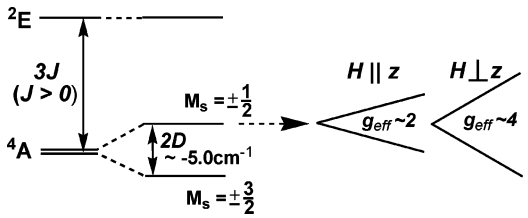

of the individual Cu sites in the trimer.[18] However, with the g_{eff} of 3.64/3.77 (X-/Q-band), the molecular $g_{x,y}$ would be 1.82/1.89, which is too low for the individual Cu centers in μ_3O. Therefore, the g_{eff} values indicate that the ZFS of the ground state is small enough that the doublets mix with applied magnetic field.

To evaluate the molecular g values and the ZFS of the ground state, simulations were performed simultaneously on the X- and Q-band EPR spectra using the spin-Hamiltonian:

$$\hat{H}_{\text{spin}} = \beta H \bar{g} \hat{S} + \hat{S} \bar{D} \hat{S} \qquad (1)$$

where β is the Bohr magneton, H is the magnetic field, $\bar{g}$ is the **g** tensor in which $g_{xx} = g_{yy} \neq g_{zz}$ and $g_{ij} = 0$ ($i \neq j$), $\hat{S}$ is the electron spin operator, and $\bar{D}$ is the **D** tensor in which $D_{xx} = D_{yy} = -{}^1/_2 D_{zz}$ ($= -D/3$) and $D_{ij} = 0$ ($i \neq j$). The best

(11) Hanson, G. R.; Gates, K. E.; Noble, C. J.; Griffin, M.; Mitchell, A.; Benson, S. *J. Inorg. Biochem.* **2004**, *98*, 903−916.
(12) Frisch, M. J.; Trucks, G. W.; Schlegel, H. B.; Scuseria, G. E.; Robb, M. A.; Cheeseman, J. R.; Zakrzewski, V. G.; Montgomery, J. A., Jr.; Stratmann, R. E.; Burant, J. C.; Dapprich, S.; Millam, J. M.; Daniels, A. D.; Kudin, K. N.; Strain, M. C.; Farkas, O.; Tomasi, J.; Barone, V.; Cossi, M.; Cammi, R.; Mennucci, B.; Pomelli, C.; Adamo, C.; Clifford, S.; Ochterski, J.; Petersson, G. A.; Ayala, P. Y.; Cui, Q.; Morokuma, K.; Malick, D. K.; Rabuck, A. D.; Raghavachari, K.; Foresman, J. B.; Cioslowski, J.; Ortiz, J. V.; Baboul, A. G.; Stefanov, B. B.; Liu, G.; Liashenko, A.; Piskorz, P.; Komaromi, I.; Gomperts, R.; Martin, R. L.; Fox, D. J.; Keith, T.; Al-Laham, M. A.; Peng, C. Y.; Nanayakkara, A.; Gonzalez, C.; Challacombe, M.; Gill, P. M. W.; Johnson, B. G.; Chen, W.; Wong, M. W.; Andres, J. L.; Head-Gordon, M.; Replogle, E. S.; Pople, J. A. *Gaussian 98*, revision A.11.3; Gaussian, Inc.: Pittsburgh, PA, 1998.
(13) (a) Baerends, E. J.; Ellis, D. E.; Ros, P. *Chem. Phys.* **1973**, *2*, 41−51. (b) Te Velde, G.; Baerends, E. J. *J. Comput. Phys.* **1992**, 99, 84−98.
(14) (a) Gorelsky, S. I. *AOMix program*, revision 6.04; http://www.sg-chem.net/. (b) Gorelsky, S. I.; Lever, A. B. P. *J. Organomet. Chem.* **2001**, *635*, 187−196.
(15) Becke, A. D. *J. Chem. Phys.* **1993**, *98*, 5648−5652.
(16) Vosko, S. H.; Wilk, L.; Nusair, M. *Can. J. Phys.* **1980**, *58*, 1200−1211.
(17) (a) Becke, A. D. *J. Chem. Phys.* **1986**, *84*, 4524−4529. (b) Perdew, J. P. *Phys. Rev. B: Condens. Matter Mater. Phys.* **1986**, *33*, 8822−8824.
(18) Pilbrow, J. R. *J. Magn. Reson.* **1978**, *31*, 479−490.

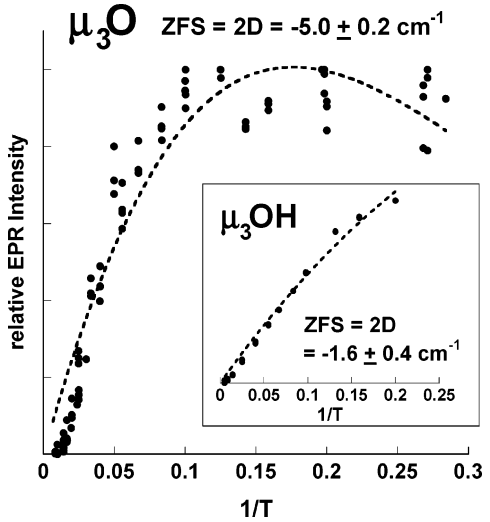

Figure 3. Boltzmann fit to the Curie law for the temperature dependence of the μ_3O powder EPR intensities arising from the transitions between $M_S = \pm^1/_2$ levels. The dotted line is a least-squares fit to the data, with ZFS of $2D = -5.0 \pm 0.2$ cm^{-1}. (Inset) Similar plot of the μ_3OH powder EPR intensities and fit curve with the ZFS of $2D = -1.6 \pm 0.4$ cm^{-1}.

simulated spectra were obtained with $g_x = g_y = 2.021$ ($\pm$ 0.010) and $g_z = 2.064$ ($\pm$ 0.005), with line width parameters $W_{x,y,z}$ = (650, 650, and 280 G) and the ZFS $D-E$ strain parameters σ_D and σ_E of 0.06 and 0.07, respectively (Figure 2). The D value could not be quantitatively obtained, but the lower limit of its magnitude is $|D| > 2.0$ cm^{-1}.

The magnitude and the sign of the D value were obtained from the temperature-dependent behavior of the EPR intensities. Figure 3 gives a plot of the normalized EPR intensities (at several fields in X-band) against $1/T$ in nonsaturating conditions. Assuming the ZFS is sufficiently large so that no transition is made between the two zero-field-split Kramer doublets of the ^{4}A ground state and that the plotted EPR intensities are purely from the transition between the $M_S = \pm^1/_2$ components, a Boltzmann fit to the Curie law dependence was performed using eq 2:

$$\text{EPR Intensity} = \frac{C}{T}\left[\frac{\exp(-2D/kT)}{1+\exp(-2D/kT)}\right] \qquad (2)$$

where C is Curie constant, T is the temperature in K, D is the axial ZFS parameter, and k is Boltzmann's constant. The best fit gives $D = -2.5 \pm 0.1$ cm^{-1}.

The energy levels are linearly dependent on field when the molecular z axis is aligned with the field but not linearly dependent when the field is perpendicular to the molecular z axis (Figure S2, Supporting Information). The nonlinearity in the latter case results from the interaction of the upper and lower doublets of the ZFS ^{4}A ground state, and this gives g_{eff} values less than 4 (Figure 2). However, the ZFS ($= 2D$) of -5.0 cm^{-1} is large enough so that no transition between the two ZFS doublets occurs with the X- or Q-band energy. This large ZFS originates from the anisotropic exchange (also called pseudo-dipolar exchange) involving the ground-to-excited superexchange interaction between an electron in the ground ($d_{z'^2}$) and the excited ($d_{x'z'}$) states (see below). The spin$-$spin dipolar contribution to ZFS is much smaller in

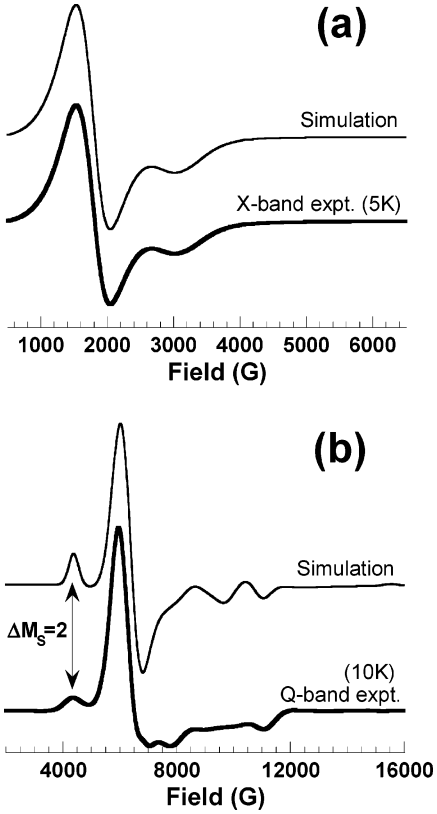

Figure 4. EPR spectra of powder μ_3OH complex and their simulations using $g_x = g_y = 2.067$, $g_z = 2.224$, $D = -1.02$ cm^{-1}, $E/D = 0$, line width parameters $W_{x,y,z}$ = (580, 580, 330 G), and the ZFS $D-E$ strain parameters σ_D and $\sigma_E = 0.05$ and 0.03, respectively. (a) X-band spectrum taken at 0.3 mW, 7.6 K, and 9.390 GHz and (b) Q-band EPR spectrum at 0.097 mW, 10.0 K, and 33.95 GHz.

magnitude ($|D_{\text{dd}}| = 0.27 \pm 0.01$ cm^{-1}) as obtained from a point dipole model in which $|D_{\text{dd}}| \approx 0.650g^2/r^3$.[19]

The calculated molecular g values from these simulations can be directly correlated to the local g values of each Cu center: $(g_x, g_y) \sim (g_{x'}, g_{z'})$ and $g_z \sim g_{y'}$, where the primed axes (x', y', and z') refer to the local coordinates of the Cu sites and the nonprimed axes (x, y, and z) refer to the μ_3O molecular coordinates with z as the direction perpendicular to the Cu_3 plane (Figure 1). The $g_z \sim g_{y'} = 2.064$ is small compared to the typical $g_\perp$ value of a trigonal pyramidal mononuclear Cu complex of ~ 2.2.[20] This is consistent with the large covalency of the Cu$-$oxo bonds. A significant orbital reduction would result in the low observed g value, as compared to those of Cu complexes with relatively weak Cu-to-ligand bonding interactions.

(b) μ_3OH. The EPR spectra of the powder μ_3OH sample taken at the X-band (9.390 GHz, 8 K) and at the Q-band (33.95 GHz, 10 K) are presented with their simulated spectra in Figure 4. The EPR signals in the X-band are observed only below 120 K, and their intensities increase as the temperature is lowered. No change in the spectral shape was observed over the temperature range of 3.65$-$120 K (Figure

(19) (a) Chasteen, N. D.; Belford, R. L. *Inorg. Chem.* **1970**, *9*, 169$-$175, 2805. (b) Chikira, M.; Kon, H.; Hawley, R. A.; Smith, K. M. *J. Chem. Soc., Dalton Trans.* **1979**, 245$-$249.
(20) Hathaway, B. J.; Billing, D. E. *Coord. Chem. Rev.* **1970**, *5*, 143$-$207.

S3, Supporting Information). In the X-band spectrum, features are observed at g_{eff} of 3.70 and 2.22, with no discernible hyperfine structure. As with μ_3O, these correspond to the "$g = 4$" and "$g = 2$" resonances of an axial ZFS quartet system with a ferromagnetic ground state, consistent with magnetic susceptibility data.[7] In the Q-band spectrum, more than two resonances are observed (Figure 4b). Here, while the "$g = 4$" and "$g = 2$" resonances are still observed at g_{eff} values of 3.75 and 2.22, additional signals are present at 4360 G ($g_{eff} \sim 5.57$) and between 8000 and 10 000 G.

Simulations were performed simultaneously on the X- and Q-band spectra using the spin Hamiltonian of eq 1. The best simulated spectra were obtained with $g_x = g_y = 2.067$ ($\pm$ 0.010) and $g_z = 2.224$ ($\pm$ 0.005), with the line width parameters $W_{x,y,z} =$ (580, 580, and 330 G) and the ZFS $D-E$ strain parameters σ_D and σ_E of 0.05 and 0.03, respectively (Figure 4). Here, the magnitude of the D value of 1.02 cm^{-1} obtained as the new signal at $g_{eff} \sim 5.57$ is very sensitive to this value. The sign of the D value could be obtained from the plot of the normalized X-band EPR intensities against $1/T$, which is presented in the inset of Figure 3. Using eq 2, the best fit gives $D = -0.8 \pm 0.2$ cm^{-1}.

As with μ_3O, the energy levels are linearly dependent on the field where the molecular z axis is aligned with the field but are not linearly dependent when the field is perpendicular to the molecular z axis (Figure S4, Supporting Information). Again, the nonlinearity of the latter case results in g_{eff} values less than 4 (Figure 4). However, the ZFS is smaller than that of μ_3O and is comparable to the Q-band energy. As a result, transitions between the doublets are observed. In particular, the $\Delta M = \pm 2$ transition that is observed at g_{eff} of 5.57 (Figure 4b) becomes allowed. The small ZFS, as compared to that of μ_3O, reflects a decreased anisotropic exchange, indicating that the ground-to-excited exchange interactions have become smaller (see below). The spin$-$spin dipolar contribution to ZFS in μ_3OH ($|D_{dd}| = 0.26 \pm$ 0.02 cm^{-1}) is, again, much smaller in magnitude than the observed ZFS of -2.04 cm^{-1}.

The molecular g_z value of 2.224 that corresponds to the g_y' of the local Cu site is similar to the typical $g_\perp$ value of a trigonal pyramidal mononuclear Cu complex. This demonstrates that the Cu$-$OH bonds in μ_3OH are much less covalent compared to the Cu$-$O bonds in μ_3O. This difference in Cu$-$O bond covalency is also reflected in the superexchange interactions in these complexes as the magnitudes of the coupling constants (e.g., isotropic exchange constant J; $+54.5$ cm^{-1} for μ_3O and $+18.9$ cm^{-1} for μ_3OH)[7] depend on the exchange integrals, which are largely related to orbital overlap.

Analysis

Spin-unrestricted DFT calculations were performed on μ_3O and its protonated form, μ_3OH, where all the ethylene groups linking N atoms in the macrocyclic ligand have been truncated with H atoms, as shown in Figure 1. Atomic labels and the axis systems used throughout the manuscript are described in Figure 1: the primed axes (x_i', y_i', and z_i') refer to the local coordinates of the ith Cu site, and the nonprimed axes (x, y, and z) refer to the molecular trimer coordinates where z is the direction perpendicular to the Cu_3 plane. These models were fully optimized in the high-spin quartet state ($\langle S^2 \rangle \approx 3.75$) at the uB3LYP/LanL2Dz level (in Gaussian 98), both resulting in C_3 symmetric structures, with the structural parameters given in Table 1 (molecular coordinates are given in Tables S1 and S2 of the Supporting Information). Overall, these optimized structures are in good agreement with the crystal structures. The geometry of each Cu site in both models is best described as a distorted trigonal bipyramidal structure which yields a d_{z^2} ground state. The calculated Cu$-$O and Cu$-$Cu distances are slightly larger than those of the experiment, likely because of the relaxed ligand structure from the truncation of the ethylene links in the original ligand system. The Cu$-$O distance in the μ_3OH model is 0.13 Å longer than that of the μ_3O model (2.10 vs 1.97 Å), which reflects the weakening of the Cu$-$O bond as a result of the protonation at the oxo ligand.

Table 1. Structural Parameters of the DFT Optimized μ_3O and μ_3OH Models[a]

	μ_3O		μ_3OH	
	expt[b]	calcd	expt[b]	calcd
R(Cu$-$Cu)	3.105/3.125	3.30	3.262/3.250	3.53
R(Cu$-$O)	1.869/1.883	1.97	1.966/1.951	2.10
R(Cu$-$N$_{ax}$)[c]	2.040/2.044	2.17	2.002/2.014	2.11
R(Cu$-$N$_B$)[c]	2.241/2.272	2.21	2.201/2.206	2.21
R(Cu$-$N$_{s1}$)[c]	2.138/2.167	2.25	2.105/2.086	2.24
R(Cu$-$N$_{s2}$)[c]	2.125/2.099	2.22	2.115/2.141	2.24
R(O$-$Cu$_3$ plane)	0.528/0.539	0.507	0.564/0.537	0.521
A(Cu$-$O$-$Cu)	112.3/112.2	113.6	112.1/112.8	114.1

[a] uB3LYP/LanL2Dz (Gaussian 98) results are presented, in which each structure resulted in C_3 symmetry. Distances are in Å, and angles are in degrees. [b] Two independent molecules are found in a unit cell.[7] [c] See Figure 1 for atomic labels.

These optimized geometries were further employed for the spin-unrestricted BP86 calculations (in ADF) using the triple-ζ Slater-type orbital basis set (ADF basis set TZP). Single-point calculations were performed in both the quartet and the broken-symmetry ($M_S = {}^1/_2$, $\langle S^2 \rangle \approx 1.75$) states. The broken-symmetry method uses the $M_S = {}^1/_2$ configurations of the trimer ($|\alpha_1\alpha_2\beta_3>$, $|\alpha_1\beta_2\alpha_3>$, $|\beta_1\alpha_2\alpha_3>$, $|\alpha_1\beta_2\beta_3>$, $|\beta_1\alpha_2\beta_3>$, or $|\beta_1\beta_2\alpha_3>$, where 1$-$3 refer to metal centers and α and β refer to up and down spins, respectively) to provide a better estimate of the multideterminant doublet state ($S_{tot} = {}^1/_2$, $\langle S^2 \rangle \approx 0.75$) energy than can be obtained from a full-symmetry calculation using the single-determinant DFT approach.[21] The relative energies of the quartet, the broken-symmetry, and the doublet states are described in Scheme 2. Accordingly, the total energy difference of the two single-determinant quartet and the broken-symmetry states can be used to estimate the isotropic exchange constant J [$= {}^1/_2(E_{BS} - E_{HS})$, where E_{BS} and E_{HS} refer to the total energy of broken-symmetry and quartet states, respectively] and, in turn, the quartet$-$doublet splitting energy $3|J|$. Table 2 gives the total energies of the μ_3O and μ_3OH models and the

(21) (a) Noodleman, L. *J. Chem. Phys.* **1981**, *74*, 5737$-$5743. (b) Noodleman, L.; Case, D. A.; Aizman, A. *J. Am. Chem. Soc.* **1988**, *110*, 1001$-$1005.

Scheme 2. Energy Splitting in the Ground State of a C_3 Symmetric Trimer with $s_1 = s_2 = s_3 = {}^1/_2$

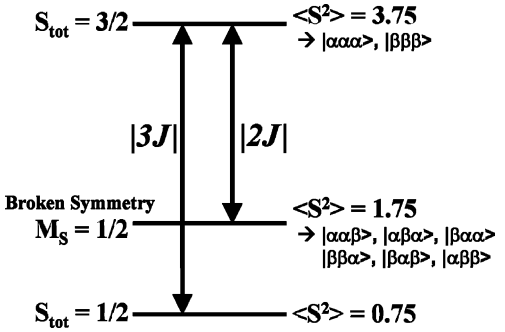

Table 2. Total Energies and Isotropic Exchange Constants (J) of the μ_3O and μ_3OH Models from DFT (ADF) Calculations[a]

	μ_3O	μ_3OH
E_{HS}[b]	−9.591 710 35 au	−9.077 810 61 au
E_{BS}[c]	−9.589 464 95 au	−9.077 596 94 au
J_{calc}[d,e]	+246.4 cm^{-1}	+23.4 cm^{-1}
J_{expt}[f]	+54.5 cm^{-1}	+18.9 cm^{-1}

[a] uBP86/TZV (ADF) results are presented. [b] The total energy (LDA + GGA + XC) of the high-spin ($S_{tot} = {}^3/_2$) state. [c] The total energy (LDA + GGA + XC) of a broken-symmetry ($M_S = {}^1/_2$) state. [d] $J = {}^1/_2(E_{BS} - E_{HS})$; refer to Scheme 2. [e] Conversion factor: 1 au = 2.194 75 × 10^5 cm^{-1}. [f] Magnetic susceptibility results.[7]

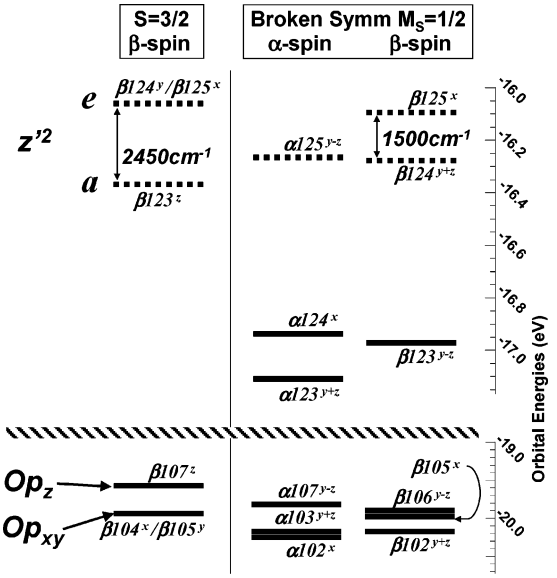

Figure 5. Energy level diagram obtained from DFT calculations on the μ_3O model, where the dotted horizontal lines indicate unoccupied spin−orbitals. Only the MOs relevant to Cu−O bonds are presented. The superscripts (x, y, and z) on the orbital numbers refer to the O p orbital involved in the indicated MO.

corresponding J values. The J's obtained indicate ferromagnetic quartet ground states for both structures, with the value for μ_3O being considerably higher, in agreement with the experimental results from EPR (above) and magnetic susceptibility.[7]

The features of the molecular orbital (MO) energy level diagram relevant to the Cu−O bonding interactions in μ_3O are presented in Figure 5 for both the quartet and the broken-symmetry states. The MOs are labeled with superscripts (x, y, and z, indicating the associated O p orbital) to facilitate the correlation between the quartet and the broken-symmetry

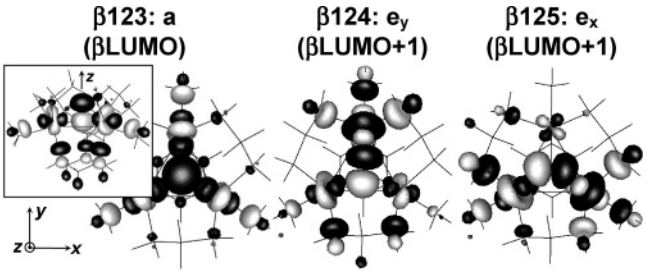

Figure 6. Contours of β-spin LUMO (β123) and LUMO+1 (β124 and β125 degenerate) obtained from DFT calculations on the μ_3O model in the high-spin state $S_{tot} = {}^3/_2$. (Inset) Side view of β123.

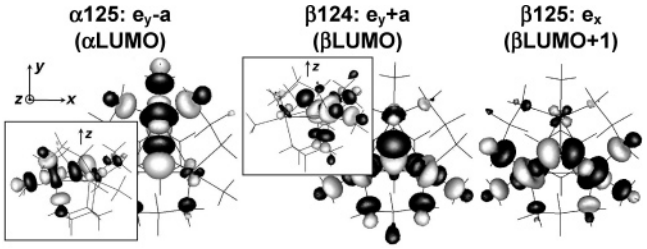

Figure 7. Contours of α- and β-spin LUMOs obtained from DFT calculations on the μ_3O model in the broken-symmetry $M_S = {}^1/_2$ state. (Insets) Side views of α125 and β124.

states. The energies and % Cu/O compositions of the MOs are listed in Tables 3 and 4. In addition, the contours of the unoccupied MOs in the high-spin and the broken-symmetry states are presented in Figures 6 and 7, respectively. In the quartet state, the MOs are categorized into four types: (1) the metal-based acceptor MO with the out-of-plane O $2p_z$-orbital character ($\beta 123^z$), (2) the metal-based acceptor MOs with in-plane O $2p_x$- or $2p_y$-orbital characters ($\beta 124^y/\beta 125^x$), (3) the donor MO based on the out-of-plane O $2p_z$ orbital ($\beta 107^z$), and (4) the donor MOs based on the in-plane O $2p_x$ and $2p_y$ orbitals ($\beta 104^x/\beta 105^y$). The MOs associated with the in-plane O p_x/p_y orbitals are degenerate with e (= e_x/e_y) symmetry in C_3 ($\beta 104^x/\beta 105^y$ and $\beta 124^y/\beta 125^x$), whereas those associated with the out-of-plane O p_z orbital are nondegenerate with a symmetry ($\beta 107^z$ and $\beta 123^z$). In the broken-symmetry state (Figure 5, right), the a and e MOs are mixed: the orbital shapes of $\alpha 123^{y+z}$, $\alpha 125^{y-z}$, $\beta 123^{y-z}$, and $\beta 124^{y+z}$ are the result of the a and e_y orbital mixing, whereas those of $\alpha 124^x$ and $\beta 125^x$ are mainly e_x. The $\alpha 125^{y-z}$ of the broken-symmetry state (Figure 7, αLUMO) is mainly localized on one metal and is useful in describing the ligand field around each Cu site. Each five-coordinated Cu^{II} site is best described by a distorted trigonal bipyramidal ligand field with the relative d-orbital energy order of $d_{z^2} \gg d_{xy} > d_{x^2-y^2} \gg d_{xz} > d_{yz}$ (Table 5). The two unoccupied β MOs of the broken-symmetry state, $\beta 124^{y+z}$ and $\beta 125^x$ (Figure 7, βLUMO and βLUMO+1), reflect the trimeric interactions in the broken-symmetry states (and, thus, the doublet state of μ_3O) and are split in energy by 1500 cm^{-1} (Figure 5, right). The Cu−O bonds in both of these β MOs are involved in strong σ interactions, as reflected by the large amount of O p-orbital character in these MOs.

The ligand-to-metal bonding interactions of the high-spin state, as described in Figure 6 and Table 3, can be used to describe the superexchange interactions present in μ_3O. The

Table 3. Energies and % Cu/O Compositions of μ_3O and μ_3OH in the High-Spin ($S_{tot} = {}^3/_2$) State

description	β-MO #	symm. in C_3	E (eV)	rel. E (cm^{-1})[a,b]	Cu_1 d_{z^2}	Cu_2 d_{z^2}	Cu_3 d_{z^2}	O 2s	O $2p_x$	O $2p_y$	O $2p_z$
					μ_3O Acceptors						
βLUMO+1	$\beta 125^x$	e	−16.06	2450	23.2	2.8[c]	27.6	0.0	19.7	0.1	0.0
βLUMO+1	$\beta 124^y$	e	−16.06	2450	12.5[d]	32.9	8.2[d]	0.0	0.1	19.7	0.0
βLUMO	$\beta 123^z$	a	−16.37	0	16.1	16.1	16.1	0.4	0.0	0.0	21.7
					μ_3O Donors						
Op_z	$\beta 107^z$	a	−19.52	−25 500	14.5	14.5	14.5	0.1	0.0	0.0	18.2
Op_x	$\beta 105^x$	e	−19.92	−28 600	7.4	10.2[c]	5.9	0.0	29.3	0.1	0.0
Op_y	$\beta 104^y$	e	−19.92	−28 600	8.3	5.5	9.7	0.0	0.1	29.3	0.0
					μ_3OH Acceptors						
βLUMO+1	$\beta 125^x$	e	−20.21	2100	24.8	1.4[c]	26.7	0.0	10.6	0.0	0.0
βLUMO+1	$\beta 124^y$	e	−20.21	2100	10.5[d]	33.9	8.6[d]	0.0	0.0	10.6	0.0
βLUMO	$\beta 123^z$	a	−20.47	0	18.4	18.4	18.4	1.1	0.0	0.0	1.0
					μ_3OH Donors						
Op_y	$\beta 93^y$	e	−25.36	−39 500	0.9	8.5	7.9	0.0	7.2	25.1	0.0
Op_x	$\beta 92^x$	e	−25.36	−39 500	10.6	3.1[c]	3.6	0.0	25.1	7.2	0.0
Op_z	$\beta 80^z$	a	−27.35	−55 600	1.1	1.1	1.1	3.9	0.0	0.0	31.9

[a] Relative energies when β-LUMO (orbital #123) is set equal to zero. [b] Conversion factor: 1 eV = 8065.54 cm^{-1}. [c] $d_{x'z'}$ character. [d] Comprises both d_{z^2} and $d_{x'z'}$ characters.

Table 4. Energies and % Cu/O Compositions of μ_3O in the Broken-Symmetry ($M_S = {}^1/_2$) State

description	MO #	E (eV)	Cu_1	Cu_2	Cu_3	O 2s	O $2p_x$	O $2p_y$	O $2p_z$
				α-Spin Acceptors					
αLUMO	$\alpha 125^{y-z}$	−16.27	2.4	48.1	2.3	0.1	3.7	11.0	3.9
αHOMO	$\alpha 124^x$	−16.94	17.2	8.0	17.4	0.0	16.0	5.6	0.0
αHOMO-1	$\alpha 123^{y+z}$	−17.11	13.9	7.3	13.8	0.0	1.1	3.0	26.0
				α-Spin Donors					
Op_z	$\alpha 107^{y-z}$	−19.83	16.3	14.3	15.7	0.2	0.4	1.0	14.3
Op_y	$\alpha 103^{y+z}$	−20.21	12.4	7.3	12.5	0.0	5.6	12.8	10.4
Op_x	$\alpha 102^x$	−20.24	6.7	9.2	6.1	0.0	21.6	6.3	0.0
				β-Spin Acceptors					
βLUMO+1	$\beta 125^x$	−16.09	26.1	1.9	25.7	0.0	14.7	4.9	0.0
βLUMO	$\beta 124^{y+z}$	−16.27	23.7	3.0	24.4	0.2	2.4	7.5	9.8
βHOMO	$\beta 123^{y-z}$	−16.96	9.1	21.1	7.4	0.0	2.7	7.7	19.2
				β-Spin Donors					
Op_z	$\beta 106^{y-z}$	−19.92	13.6	13.9	14.2	0.0	0.3	2.6	13.6
Op_x	$\beta 105^x$	−19.95	8.0	12.7	6.0	0.0	16.7	5.3	0.1
Op_y	$\beta 102^{y+z}$	−20.15	8.3	7.8	8.1	0.0	5.3	17.3	3.2

Table 5. d orbital Energies of μ_3O and μ_3OH[a]

	μ_3O		μ_3OH	
	E (eV)	rel. E (cm^{-1})	E (eV)	rel. E (cm^{-1})
d_{z^2}	−16.3	0	−20.3	0
$d_{x'y'}$	−17.6	10 500	−21.5	9680
$d_{x^2-y^2}$	−18.0	13 700	−21.9	12 900
$d_{x'z'}$	−18.7	19 400	−22.6	18 600
$d_{y'z'}$	−19.0	21 800	−22.8	20 200

[a] Orbital energies of the α MOs obtained from the broken-symmetry calculations using ADF.

Cu sites have dominantly the d_{z^2} ground state forming either σ or pseudo-σ antibonding MOs with the O 2p orbitals. In the quartet ground state ($S_{tot} = {}^3/_2$ in Figure 5), the degenerate $\beta 124^y$ and $\beta 125^x$ have considerable in-plane O $2p_y$ and $2p_x$ character (20% each, Table 3), respectively, reflecting strong oxo σ bonds with the metal d_{z^2} orbitals. The nondegenerate $\beta 123^z$ contains the out-of-plane O $2p_z$ (22%, Table 3) that forms pseudo-σ bonds with all three metal d_{z^2} orbitals as a consequence of the oxo being out of the Cu_3 plane by ~0.5 Å. The pseudo-σ bonds in the a MO (= βLUMO) lead to its destabilization. Consequently, the energy gap between the a and e (= βLUMO+1) acceptor MOs is reduced, and the resulting energy gap of 2450 cm^{-1} (Figure 5, left) is small enough for the ferromagnetic contribution to dominate over the antiferromagnetic contribution, leading to a quartet ground state (see below). Note also that the symmetries of $\beta 124$ and $\beta 125$ MOs (Figures 6 and 7) suggest that the d_{xz} excited-state orbitals should have π-type bonds with the in-plane oxo p orbitals. These bonds would provide effective ground-to-excited superexchange interactions that lead to higher-order exchange interactions, in particular, anisotropic exchange, which yields a ZFS of −5.0 cm^{-1} in the ^{4}A ground state of μ_3O (see below).

The contours of the unoccupied β-spin acceptor MOs of the protonated μ_3OH model in the high-spin quartet state are presented in Figure 8; their orbital energies and % MO compositions are listed in Table 3. The energy gap between the a (= βLUMO) and the e MOs (= βLUMO+1) is similar to that of μ_3O [2450 cm^{-1} (μ_3O) vs 2100 cm^{-1} (μ_3OH)], and as a consequence, the ground state of μ_3OH is also a ferromagnetic quartet state (Table 2). However, a considerable reduction of both the σ and pseudo-σ interactions between Cu−O bonds is found: in the $\beta 124^y/\beta 125^x$ e MOs, the in-plane O $2p_y/2p_x$ characters are reduced by half (from 20 to 11% each; Table 3), and in the $\beta 123^z$ a MO, the out-of-plane O $2p_z$ character is essentially eliminated (from 22

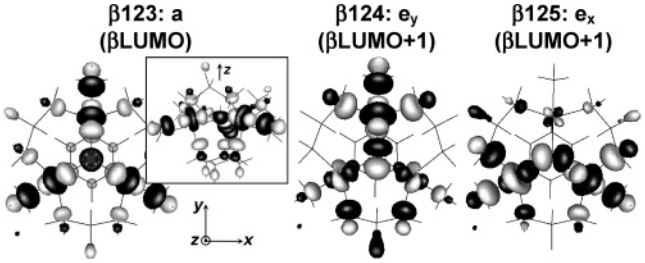

Figure 8. Contours of β-spin LUMO and LUMO+1 (β124 and β125 degenerate) obtained from DFT calculations on the μ_3OH model in the high-spin state $S_{tot} = {}^3/_2$. (Inset) Side view of β123.

to 1%; Table 3). Moreover, the magnitude of the calculated ferromagnetic J for μ_3OH is considerably reduced as compared to that of μ_3O (Table 2). This decrease in J is due to the reduction of the ferromagnetic contribution; the decreased oxo characters in the *a* and *e* MOs represent the reduction of the spin density overlap between the orthogonal magnetic orbitals.[22] Alternatively, the antiferromagnetic contribution remains virtually unaffected since the energy gap between the βLUMO and βLUMO+1 is similar to that of μ_3O, as both of these MOs are shifted in energy by a similar amount from decreased Cu−O interactions due to protonation.

Note that because of the decrease in the Cu−O interactions in μ_3OH (between the Cu d_{z^2} and the O $p_{x,y,z}$ orbitals), the energy gap between the d_{z^2} ground state and the rest of the d manifold is reduced relative to that of the μ_3O model (Table 5). This is experimentally observed in absorption and MCD spectra in which the d−d transition energies are lower for μ_3OH.[23] The effect of protonation is also reflected in the large stabilization of the O-based donor MOs, which are lowered in orbital energy by 10 800 cm^{-1} (Op_x/Op_y) and 27 300 cm^{-1} (Op_z) relative to the LUMOs, resulting in the large increase in energy of the associated charge-transfer transitions.[23]

Finally, the effect of the position of the oxo ligand relative to the Cu_3 plane on the superexchange interaction was evaluated by varying the oxo-to-Cu_3 plane distance.[24] Table 6 lists the resulting structural parameters, orbital energies of the βLUMO and βLUMO+1 of the high-spin state, J values, and the % MO compositions of the magnetic orbitals obtained from the broken-symmetry calculations. The most conspicuous feature found in these calculations is that the J's vary significantly from −100 to +285 cm^{-1} and that the antiferromagnetic ground state is favored when the distance of the oxo ligand out of the Cu_3 plane, R(O−Cu_3 plane), is smaller than 0.3 Å, while the ferromagnetic ground state is favored when R(O−Cu_3 plane) is larger than 0.3 Å (Figure 9a).[25] This variation in J is not related to either the Cu−Cu/Cu−O distances or the Cu−O−Cu bridging angles, as these parameters do not significantly change over the different R(O−Cu_3 plane) values.

In particular, the Cu−O−Cu bridging angles, typically used as a criterion for assessing the magnetic properties of dimeric Cu^{II} complexes, appear to play less of a role for μ_3O, as the angles obtained of 108.6°−120.0° (Table 6a) are in the range that would generally favor a large antiferromagnetic interaction in dimeric Cu^{II} complexes; the Cu−O−Cu angles of ∼112° in the μ_3O crystal structure correspond to a strongly antiferromagnetic J of ∼−500 cm^{-1}.[26] This difference between dimers and the μ_3-oxo trimers is related to the fact that the antiferromagnetic contribution in Cu^{II} dimers depends on the bonding interactions between the Cu d and the in-plane OH p orbitals in the singly occupied MO (SOMO) and SOMO+1; the OH p_y and p_x orbitals (perpendicular and parallel to the Cu−Cu direction, respectively) each form two Cu−O bonds in the SOMO and SOMO+1. The dependence of J on the Cu−O−Cu angle for the Cu^{II} dimers is, thus, a consequence of the difference in the in-plane d−p_y−d and d−p_x−d overlaps. However, for the μ_3O trimer, the high-spin SOMO and the degenerate SOMO+1 (βLUMO and βLUMO+1; Figure 6) involve the out-of-plane O p_z orbital and the in-plane O $p_{x,y}$ orbitals, respectively, and therefore, the two-dimensional Cu−O−Cu angle is not sufficient for assessing exchange interactions in μ_3O.

In contrast to the effect of protonation described above, the ferromagnetic contribution, which is largely dependent on the contribution of orthogonal magnetic orbitals to a single center (i.e., oxo), is expected to be unaffected, as the oxo characters in the magnetic orbitals remain relatively invariant at different R(O−Cu_3 plane) distances (Table 6c). Alternatively, the energy gap ($E_{\beta LUMO} - E_{\beta LUMO+1}$) becomes large when J becomes small. This reciprocal nature of J and $E_{\beta LUMO+1} - E_{\beta LUMO}$ has been recognized by Hay et al.[27] According to their model, J has a linear relationship with the SOMO−SOMO+1 energy gap squared, assuming the ferromagnetic contribution remains constant.[27]

The calculated J's and the corresponding $(E_{\beta LUMO+1} - E_{\beta LUMO})^2$ are plotted in Figure 9b, in which a linear fit is obtained with a ferromagnetic contribution of +335 cm^{-1} and an antiferromagnetic contribution of $-(E_{\beta LUMO+1} - E_{\beta LUMO})^2/85\,900$ cm^{-1}. The denominator in the latter term (85 900 cm^{-1} ∼ 10.5 eV) is reasonable, as this energy is the energy of the metal-to-metal charge transfer (MMCT) state, which is related to the Coulomb repulsion energy of the paired electrons in the MMCT state and has been estimated

(22) Kahn, O.; Galy, J.; Journaux, Y.; Jaud, J.; Morgenstern-Badarau, I. *J. Am. Chem. Soc.* **1982**, *104*, 2165−2176.

(23) Yoon, J.; Mirica, L. M.; Stack, T. D. P.; Solomon, E. I. *J. Am. Chem. Soc.* **2005**, in press.

(24) The geometry optimizations [using uB3LYP/LanL2Dz in the high-spin ($S_{tot} = 3/2$) state; Gaussian 98] were performed on the μ_3O model at six different oxo-to-Cu_3 plane distances. C_{3v} symmetry was imposed on these optimizations, which showed no significant deviation in geometry from the C_3 symmetry optimized structure [compare Table 1 and R(O−Cu_3 plane) = 0.504 Å in Table 6a].

(25) The difference in the calculated J values in Table 2 (+246.4 cm^{-1}) and those in Table 6 [+184.0 cm^{-1}; R(O−Cu_3 plane) = 0.504 Å] originates from the different functionals and basis sets used, not likely from the two geometry optimizations, as the two geometries are very similar.

(26) (a) Kahn, O. *Molecular Magnetism*; VCH: New York, 1993. (b) Crawford, V. H.; Richardson, H. W.; Wasson, J. R.; Hodgson, D. J.; Hatfield, W. E. *Inorg. Chem.* **1976**, *15*, 2107−2110. (c) Tandon, S. S.; Thompson, L. K.; Manuel, M. E.; Bridson, J. N. *Inorg. Chem.* **1994**, *33*, 5555−5570.

(27) Hay, P. J.; Thibeault, J. C.; Hoffmann, R. *J. Am. Chem. Soc.* **1975**, *97*, 4884−4899.

Table 6. (a) Structural Parameters, (b) Orbital Energies and the Isotropic Exchange Constant J's, and (c) Compositions of the Magnetic Orbitals Localized at a Single Cu Site in μ_3O at Different Oxo-to-Cu_3 Plane Distances[a]

R(O−Cu_3 plane)	0.0	0.1	0.2	0.3	0.504[b]	0.7
			(a) Structural Parameters[c,d]			
R(Cu−Cu)	3.33	3.33	3.33	3.32	3.30	3.27
R(Cu−O)	1.92	1.93	1.93	1.94	1.97	2.01
R(Cu−N_{ax})	2.14	2.14	2.15	2.16	2.18	2.20
R(Cu−N_B)	2.35	2.39	2.26	2.24	2.21	2.20
R(Cu−$N_{s1,s2}$)	2.23	2.24	2.24	2.24	2.24	2.23
A(Cu−O−Cu)	120.0	197.7	118.9	117.7	113.7	108.6
			(b) Energies[d]			
$E_{\beta LUMO+1}$ (eV)	−14.64	−14.55	−14.56	−14.60	−14.72	−14.87
$E_{\beta LUMO}$ (eV)	−15.33	−15.33	−15.30	−15.24	−15.15	−15.11
$E_{\beta LUMO+1} - E_{\beta LUMO}$ (cm^{-1})	5570	6290	5970	5160	3470	1940
J (cm^{-1})	−55.2	−100.1	−51.2	+28.8	+184.0	+285.4
			(c) Compositions of the Magnetic Orbitals[e] (%)			
Cu_2 (d_{z^2})[f]	62.0	61.9	61.6	61.4	60.9	60.2
O ($p_z + p_{x,y}$)	13.1	13.2	13.8	14.4	15.6	16.9

[a] uB3LYP/LanL2Dz (Gaussian 98) results are presented. Each structure was optimized in C_{3v} symmetry at the high-spin quartet ($S_{tot} = {}^3/_2$) state. Distances are in Å, and angles are in degrees. [b] R(O−Cu_3 plane) obtained when it was not fixed. [c] See Figure 1 for atomic labels. [d] βLUMO and βLUMO+1 refer to the unoccupied β108 and β109/β110 MOs of the high-spin calculations, respectively. [e] αLUMO (α110) of the broken-symmetry ($M_S = {}^1/_2$) calculation. [f] Compositions of the other two Cu centers in the trimer (Cu_1 and Cu_3) are less than 1%.

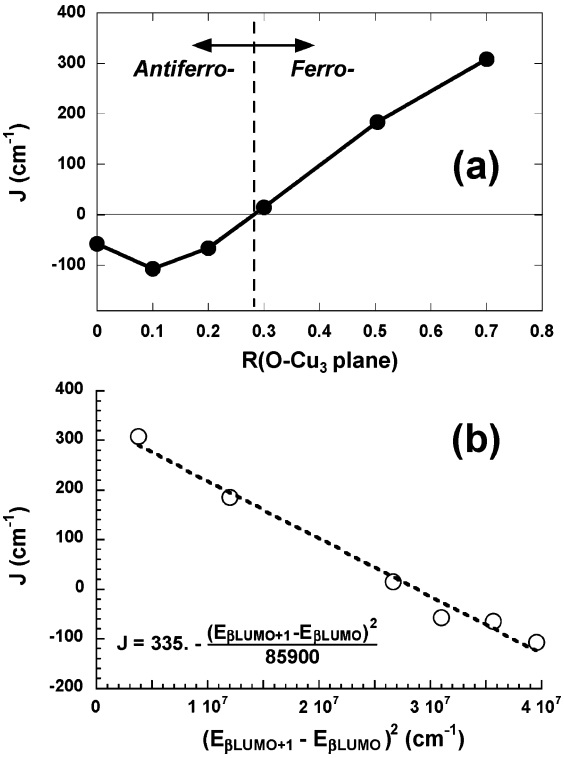

Figure 9. (a) Plot of the isotropic coupling constant J's at different oxo-to-Cu_3 plane distances, R(O−Cu_3 plane) and (b) the linear correlation between these J's and the corresponding $(E_{\beta LUMO+1} - E_{\beta LUMO})^2$ energy gap, as obtained from DFT calculations. Refer to Table 6 for more details.

to be in the range of 5−10 eV.[28,29] Thus, change in the exchange coupling interaction when the oxo ligand is moved into the Cu_3 plane is dominantly dependent on the change in the antiferromagnetic contribution that is determined by the energy gap between βLUMO and βLUMO+1. When the oxo ligand is moved out of the Cu_3 plane, the pseudo-σ overlap between Cu d_{z^2} and the out-of-plane oxo p_z orbitals increases. Consequently, the antibonding βLUMO (the *a* MO; Figure 6) is destabilized and its energy gap with βLUMO+1 (the *e* MO; Figure 6) is decreased and, thus, reduces the antiferromagnetic contribution relative to the ferromagnetic contribution. This results in the experimentally determined J of +54.5 cm^{-1} for the μ_3O complex in which the R(O−Cu_3 plane) is ∼0.5 Å. Conversely, moving the oxo ligand into the Cu_3 plane [R(O−Cu_3 plane) < 0.3 Å] results in an antiferromagnetically coupled system due to loss of the pseudo-σ interactions in the βLUMO that leads to its decreased destabilization and increased $(E_{\beta LUMO+1} - E_{\beta LUMO})$ energy gap.

Discussion

In this study, experimental and computational perturbations on the μ_3O structure, protonation of the oxo ligand, and variation of the oxo-to-Cu_3 plane distance have been performed to evaluate the behavior of the μ_3-oxo bridging ligand in the exchange coupling of the three Cu^{II} centers in the μ_3O complex. DFT analysis has shown that the difference in the magnitude of J between μ_3O and its protonated form, μ_3OH, arises from the large decrease in the Cu^{II}−oxo bonding interactions upon protonation. Consequently, the ferromagnetic contribution to the exchange coupling is reduced, which reflects the decrease in the spin density contributions from the orthogonal magnetic orbitals of the three metal centers to the bridging ligand. However, the $(E_{\beta LUMO+1} - E_{\beta LUMO})$ energy gap, and hence, the antiferromagnetic contribution, shows little change upon protonation as both orbitals are stabilized in energy by the reduced Cu−O bonding interactions. Alternatively, upon moving the oxo ligand close to the Cu_3 plane, the antiferromagnetic contribution is greatly increased and dominates over the relatively constant ferromagnetic contribution. This is a consequence of the reduction of the pseudo-σ bonding interactions between the Cu d_{z^2} and the out-of-plane oxo p_z orbitals, which increases the βLUMO and βLUMO+1 energy splitting. With

(28) (a) Anderson, P. W. *Phys. Rev.* **1959**, *115*, 2−13. (b) Anderson, P. W. In *Magnetism*; Rado, G. T., Suhl, H., Eds.; Academic Press: New York, 1963; Vol. 1, pp 25−83.
(29) Didziulis, S. V.; Cohen, S. L.; Gewirth, A. A.; Solomon, E. I. *J. Am. Chem. Soc.* **1988**, *110*, 250−268.

the decrease of the $d_{z^2}-p_z$ interactions, the ground state of μ_3O becomes an antiferromagnetic ^{2}E state when the oxo-to-Cu_3 plane distance is less than ~0.3 Å. Note that the trinuclear Cu cluster site in the MCOs is less rigid than the bowl-shaped macrocyclic ligand of μ_3O. Therefore, if the trinuclear Cu cluster site in the NI of the MCOs has a μ_3-oxo-bridged structure, the central oxo ligand would likely be positioned close to the Cu_3 plane (from QM/MM geometry optimization of NI),[30] resulting in a spin-frustrated doublet ground state, as observed experimentally.[2]

The orbitally degenerate ^{2}E ground state of an antiferromagnetically coupled μ_3O would zero-field split by the first-order antisymmetric exchange.[31] This exchange can be related to the large ZFS in the ferromagnetic ^{4}A ground state of μ_3O that has been experimentally determined here from VT EPR. The ZFS of the ^{4}A state is governed by the anisotropic exchange (D), which derives from second-order SOC combined with ground-to-excited-state exchange coupling.[31] Importantly, the anisotropic exchange shares the same physical origin as the antisymmetric exchange (G). For a pair of metal centers, these exchange terms are expressed as

$$G_{12} = 2i\lambda\left[\frac{\langle e_1|L_1|g_1\rangle}{\Delta_1}(-2J^{e_1g_2}_{g_1g_2}) - \frac{\langle e_2|L_2|g_2\rangle}{\Delta_2}(-2J^{g_1e_2}_{g_1g_2})\right] \quad (3)$$

$$D_{12} = \lambda^2\left[\frac{\langle e_1|L_1|g_1\rangle^2}{{\Delta_1}^2}(-2J^{e_1g_2}_{e_1g_2}) + \frac{\langle e_2|L_2|g_2\rangle^2}{{\Delta_2}^2}(-2J^{g_1e_2}_{g_1e_2})\right] \quad (4)$$

where λ is the SOC parameter; $|g_i>$ and $|e_i>$ are the ground and excited states at the ith metal center; Δ_i is the energy difference between $|g_i>$ and $|e_i>$; L_i is the orbital angular momentum operator that couples $|g_i>$ and $|e_i>$; and $J^{e_1g_2}_{g_1g_2}$, $J^{g_1e_2}_{g_1g_2}$, $J^{e_1g_2}_{e_1g_2}$, and $J^{g_1e_2}_{g_1e_2}$ are superexchange integrals[32] in which $J^{e_1g_2}_{g_1g_2}$ involves the transfer of one electron in the ground state of metal 1 to the ground state of metal 2 and the second electron from the ground state of metal 2 to the excited state of metal 1, while $J^{e_1g_2}_{e_1g_2}$ involves the transfer of both electrons between the excited state of metal 1 and the ground state of metal 2. Thus, both the antisymmetric and anisotropic exchanges are derived from (1) local SOC and (2) superexchange coupling between the ground state of one center to the excited state of the other center, and vice versa.

Scheme 3. Ground (d_{z^2}) to Excited (d_{xz}) State SOC and Superexchange Pathways in μ_3O

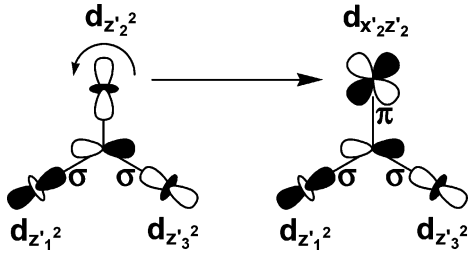

In the μ_3O structure, the d_{z^2} ground state at each metal center can SOC with the d_{xz} excited state via orbital angular momentum operator $L_{y'} \sim L_z$ (local y' axis ~ molecular z axis; Figure 1).[33] Further, the ground-to-excited-state superexchange between d_{z^2} and d_{xz} orbitals of different metal centers is facilitated via the in-plane oxo p orbitals as superexchange pathways (Scheme 3). The ZFS of -5.0 cm^{-1} in the ^{4}A ground state in μ_3O, dominated by the anisotropic exchange contribution (the spin−spin dipolar contribution being less than ~0.3 cm^{-1}), provides experimental evidence, in magnitude and sign, for the existence of the combined effects of the local SOC and ground-to-excited-state superexchange. Therefore, it is expected that the ^{2}E ground state of the μ_3O structure would also undergo ZFS by the antisymmetric exchange interaction. The ground-to-excited exchange integral $J^{xz_1z_2^2}_{z_1^2z_2^2}$ should be larger than the ground-to-ground exchange integral $J^{z_1^2z_2^2}_{z_1^2z_2^2}$, as the ground-to-excited antiferromagnetic coupling is further facilitated by the π bond between d_{xz} and the in-plane oxo p orbital which σ-bonds to d_{z^2} on the adjacent Cu centers, as illustrated in Scheme 3. Using the calculated ground-state exchange coupling constant $J^{z_1^2z_2^2}_{z_1^2z_2^2}$ of -55.2 cm^{-1} [= J when R(O−Cu_3 plane) is 0 Å; Table 6] as a lower limit for $J^{xz_1z_2^2}_{z_1^2z_2^2}$, the magnitude of the pairwise antisymmetric exchange parameter $|G_{12}|$ of 42 cm^{-1} can be estimated.[34] Thus, the ^{2}E ground state of μ_3O with the oxo ligand in the Cu_3 plane would exhibit a ZFS of ~70 cm^{-1} ($=\sqrt{3}|G_{12}|$ for the Cu^{II}_3 trimer)[6] from the antisymmetric exchange.

(30) Rulíšek, L.; Solomon, E. I.; Ryde, U. *Inorg. Chem.* **2005**, *44*, 5612−5628.

(31) Matrices obtained upon application of the spin wave functions of an axial C_3 symmetric trimer with $s_1 = s_2 = s_3 = {}^1/_2$ to the spin-Hamiltonian describing isotropic, antisymmetric, and anisotropic exchange terms are given in the Supporting Information. It is shown that only the antisymmetric exchange exists in the ^{2}E state, whereas only the anisotropic exchange exists in the ^{4}A state.

(32) These exchange integrals can be explicitly written as

$$J^{e_1g_2}_{g_1g_2} = \langle \phi_g{}^1(1)\phi_g{}^2(2)|\hat{H}_{ex}|\phi_e{}^1(2)\phi_g{}^2(1)\rangle \quad (a)$$

$$J^{g_1e_2}_{g_1g_2} = \langle \phi_g{}^1(1)\phi_g{}^2(2)|\hat{H}_{ex}|\phi_g{}^1(2)\phi_e{}^2(1)\rangle \quad (b)$$

$$J^{e_1g_2}_{e_1g_2} = \langle \phi_e{}^1(1)\phi_g{}^2(2)|\hat{H}_{ex}|\phi_e{}^1(2)\phi_g{}^2(1)\rangle \quad (c)$$

$$J^{g_1e_2}_{g_1e_2} = \langle \phi_g{}^1(1)\phi_e{}^2(2)|\hat{H}_{ex}|\phi_g{}^1(2)\phi_e{}^2(1)\rangle \quad (d)$$

in which the superscripts 1 and 2 refer to the metal centers and 1 and 2 in the parentheses refer to electrons. The exchange Hamiltonian $\hat{H}_{ex}$ includes contributions from both the two-electron Coulomb operator $1/r_{12}$ and the superexchange derived from metal−ligand overlaps.

(33) Each metal pair in μ_3O has an effective 2-fold rotation axis passing through the midpoint of the pair, with the axis nearly in the Cu_3 plane. The symmetry rules of the **G** vectors allow the nonzero G component to be oriented perpendicular to the 2-fold axis. The collection of these components from the three metal pairs results in $G_z \neq 0$ and (G_x, G_y) ≈ 0. Since (G_x, G_y) ≈ 0, exchange interactions between other orbital states (via L_x and L_y) would have negligible contributions in the antisymmetric exchange interaction.

(34) If only the d_{z^2} ground to d_{xz} excited-state SOC is considered, eq 3 can be written as

$$G_{12} = \frac{4i\lambda\langle x'z'_1|L_{1y'}|z'_1{}^2\rangle}{(-2J^{xz_1z_2^2}_{z_1^2z_2^2})} \quad (e)$$

since $\langle x'z'_1|L_{1y'}|z'_1{}^2\rangle = -\langle x'z'_2|L_{2y'}|z'_2{}^2\rangle$ (see ref 3 for details). Substituting $\langle x'z'_1|L_{1y'}|z'_1{}^2\rangle = i\sqrt{3}$, $\Delta_1 = 15\,000$ cm^{-1} (from absorption/MCD; see ref 23), the λ (SOC constant for Cu^{II}) = -830 cm^{-1}, and $J^{xz_1z_2^2}_{z_1^2z_2^2} = -55.2$ cm^{-1}, $G_{12} = 42.3$ cm^{-1} is obtained. Note that the two-center G_{12} is a vector component along the $y' \sim$ molecular z axis. The effective sum of the three two-center G_{12}'s in the symmetric trigonal systems equal $\sqrt{3}G_{12} = 73.3$ cm^{-1}.

A similar ZFS of 65 cm^{-1} has been experimentally determined in the ^2E ground state of TrisOH, which results from the combined effects of symmetry lowering and antisymmetric exchange (see the Introduction).[3] We have used a spin-Hamiltonian model to show that the antisymmetric exchange SO mixes the two ZFS doublets of the ^2E ground state, resulting in low g_{eff} values which shift down to <1.2 in the perpendicular direction (i.e., when the molecular z axis normal to the Cu_3 plane is oriented perpendicular to the magnetic field).[3,6] This model is appropriate for any antiferromagnetically coupled Cu^{II} trimer with near C_3 symmetry, as it does not take into account the specific orbital superexchange pathways involved. Thus, an antiferromagnetically coupled μ_3O structure is also expected to produce low g values in the perpendicular direction, as it has efficient ground-to-ground and ground-to-excited-state superexchange pathways for antisymmetric exchange.

Therefore, both the μ_3-oxo-bridged and the tris-μ_2-hydroxy-bridged structures would exhibit an unusual $S = {}^1/_2$ EPR signal with low g values below 2.0. The characteristic EPR signal of NI, which exhibits a low g_{eff} value of $\sim$1.65, can be explained by $\sim$6% SO mixing[35] between the ground and the low-lying excited doublet states via antisymmetric exchange among the three Cu^{II} centers in the trinuclear cluster site. The fundamental description of the ground state of the exchange coupled μ_3-oxo-bridged structure in this study and that of the tris-μ_2-hydroxy-bridged TrisOH in ref 3 allow detailed insight into the nature of the ground state of the native intermediate. This is important with respect to both the molecular mechanism of O−O bond cleavage and the contribution of the superexchange pathways to the facile rereduction of this fully oxidized intermediate in the turnover of the multicopper oxidases.

Acknowledgment. We thank A. Dey for helpful discussions regarding synthesis of the μ_3O model. This research was supported by NIH Grant DK31450.

Supporting Information Available: Structure of the macrocyclic ligand; temperature dependence of powder X-band EPR spectra and the Zeeman split energy level diagrams of μ_3O and μ_3OH; the molecular coordinates of the truncated models used in the DFT calculations; and the matrix elements of the isotropic, antisymmetric, and anisotropic exchange for a C_3-symmetric trimer with $s_1 = s_2 = s_3 = {}^1/_2$. This material is available free of charge via the Internet at http://pubs.acs.org.

IC0507870

(35) The theoretical model used for TrisOH[3] included symmetry lowering δ [an equilateral ($J_{12} = J_{23} = J_{31}$ and $\delta = 0$) to isosceles ($J_{12} \neq J_{23} = J_{31}$ and $\delta = J_{12} - J_{23}$) distortion] and antisymmetric exchange factor G ($\approx G_z$), which were varied to match the experimental data ($g = 2.15$, 1.86, and 1.65 and ZFS = 150 cm^{-1}).[2] The experimental g value of 2.15 was assumed to be g_{eff} when the molecular z axis (the axis normal to the Cu_3 plane) is aligned with the applied magnetic field, and the g values of 1.86 and 1.65 were assumed to be g_{eff} when the molecular z axis was oriented perpendicular to the applied field. The data were fit by fixing the molecular g_z at 2.15 (= highest g value from experiment) and the molecular $g_{x,y}$ at 2.0; the latter was chosen after several initial trials (small variation from 2.0 had a negligible influence on the fits). δ was varied and G was obtained from the relation $\Delta(\mathrm{ZFS}) = \sqrt{\delta^2 + 3G^2} = 150$ cm^{-1}, from which $\delta = 132 \pm 8$ cm^{-1} and $G = 41 \pm 8$ cm^{-1} were obtained. Given these values, the coefficient of mixing of the low-lying excited doublet state into the ground doublet state (or of the ground doublet state into the low-lying excited doublet state) is obtained from the expression $(\sqrt{1/2(1-\delta/\Delta)})^2 = 6.2\ (\pm 2.5)$ %.